5.2 SUPERSATURATION VARIATIONS AMONG DROPLET TRAJECTORIES THROUGH A WARM CUMULUS: EFFECTS ON DROPLET SIZE DISTRIBUTIONS

Sonia Lasher−Trapp*
New Mexico Institute of Mining and Technology, Socorro, New Mexico

William A. Cooper
National Center for Atmospheric Research♦, Boulder, Colorado

Alan M. Blyth
University of Leeds, Leeds, United Kingdom

1. INTRODUCTION

A long−standing problem in cloud microphysics is that droplet size distributions calculated in models are usually narrower than those observed in clouds. While it is generally understood that this discrepancy arises from the effects of entrainment, this relationship has not been tested in a quantitative manner. This paper seeks to develop the framework for such a quantitative test.

Cooper (1989) argued that broadening of the drop size distribution during condensation can occur if the integral radius, vertical velocity, or their correlation vary along different trajectories that contribute to the measured drop size distribution. However, this variation must occur in a way that breaks the link between supersaturation and vertical wind, because otherwise droplets would grow to an altitude−dependent size (Bartlett and Jonas 1972). Entrainment breaks this connection and introduces the possibility for independent variations in integral radius and vertical velocity. The variability along trajectories arises from random turbulent motions: Just as droplets in one region of the cloud (perhaps extending over 100 m, as for many in situ measurements) will diffuse apart in time, so they must have experienced randomly varying trajectories before arriving at that region of the cloud. As a result, individual droplets can experience different supersaturation histories and so may grow to different sizes.

The present study investigates such time−averaged variations of supersaturation along trajectories in a simulated 3D cumulus cloud and their effect on the drop size distribution produced by condensation. The cloud simulation represents a particular cloud that was observed on 22 July 1995 during the Small Cumulus Microphysics Study (SCMS), but it can also represent any moderately−sized, turbulent cumulus cloud.

2. MODELING FRAMEWORK

2.1 *3D Cloud Simulation and Trajectories*

The backdrop for the condensation calculations is the cumulus congestus modeled in three dimensions with high spatial resolution (50 m) from Lasher−Trapp et. al (2001). The cloud was modeled using the nested−grid version of the Straka Atmospheric Model as adapted by Carpenter et al. (1998). This model uses prognostic equations for the three velocity components, pressure, potential temperature, water vapor and cloud water, and subgrid−scale turbulent kinetic energy. The cloud water results from conversion of water vapor according to the bulk condensation scheme of Soong and Ogura (1973), and no autoconversion of cloud water to rain water is permitted. The details of entrainment in the model are represented by reducing the water vapor at a grid point according to the advection and diffusion of dry air from outside the cloud, solving for the new temperature and subsaturation simultaneously (accounting for the future amount of evaporation), and then evaporating the existing cloud water at that point until saturation is reached again or until all the cloud water is depleted.

The cloud is initiated by a Gaussian−shaped heat flux near the surface added to a conditionally unstable atmosphere represented by the 22 July 1545 UTC sounding from the SCMS. The environmental wind is set to zero throughout the domain, but a small random velocity perturbation (max 0.2 m s^{-1}) is initialized in the boundary layer. The cloud starts as a smooth, dome−shaped thermal that modifies into a turbulent cumulus congestus. The cloud lifetime is approximately 20 min; cloud base and max cloud top height are 1050 and 5000 m, respectively.

The simulated cloud provides air trajectories, and dynamic and thermodynamic quantities along the trajectories, such as updraft speed, pressure, temperature and total water mixing ratio (vapor + condensate). These variables reflect the entrainment and mixing occurring in the simulation, and constrain the drop calculations as described in Section 2.2.

The trajectories are calculated from the simulated cloud fields by making some assumptions about the subgrid−scale turbulence. At a chosen "source point" in the simulated cloud, the trajectories are run backward to

* *Corresponding author address*: Sonia Lasher−Trapp, NCAR/ASP, P.O. Box 3000, Boulder, CO 80307−3000; email: slasher@ucar.edu

♦NCAR is sponsored by the National Science Foundation.

below cloud base. The trajectories are calculated using the cloud model velocities $\mathbf{v}_i$ with the addition of random components $\delta\mathbf{v}_i$, from

$$\delta x_i = -(v_i + \delta v_i)\Delta t$$

where i= 1,2,3 for the three spatial dimensions and corresponding velocity components and Δt= 5 s. The quantity $\delta\mathbf{v}$ is a representation of the effect of the subgrid−scale turbulence. The cloud model contains a prognostic equation for the sub−grid scale turbulent kinetic energy, E, based on the 1−1/2 order closure scheme of Klemp and Wilhelmson (1978) which includes source terms for buoyancy and shear and a sink term for dissipation and assumes that the model grid spacing is within the inertial subrange. At each point along the trajectory, a random velocity δv is calculated from

$$\delta v_j = f\alpha_j + (1-f)\delta v_{j-1} \quad ,$$

where α_j is a random velocity generated by a Gaussian random number generator to have zero mean and standard deviation equal to $\sqrt{2E/3}$. To preserve the integral time scale τ of the turbulent motions, *f* is chosen to be $f = \Delta t/\tau$. The integral time scale is calculated from

$$\tau = \frac{\Delta}{(2\pi)^{1/3}}\left(\frac{C}{E}\right)^{1/2}$$

where Δ is the model grid spacing (50 m), C=1.5 (for isotropic turbulence) and E is the cloud model value of turbulent kinetic energy interpolated to the present location along the trajectory. As a result, when the model−calculated subgrid−scale turbulent kinetic energy (E) is large, τ is small and the new random velocity will be less correlated with the previous one. Conversely, when E is small, τ is large so the new random velocity will be more correlated with the previous value. The value of *f* is constrained to be ≤ 1. Calculations based on this algorithm show that along a trajectory E may vary from ~ 0.02 to 4.0 $m^2\ s^{-2}$, corresponding to integral time scales ~15 to 235 s. These values are consistent with the conclusions of Rodi (1981), whose data for integral scale lengths suggest integral time scales of order 100 s in the early stages of cumulus development.

2.2 *Condensation Model*

The condensation model of Cooper et al. (1997) is used to grow size distributions of drops along each trajectory. The model is initialized at each trajectory location at cloud base with the 22 July SCMS observed CCN spectrum expressed as a CS^k relation with C= 1114 and k= 0.77. Intermediate and larger sizes of CCN are as specified in Cooper et al. (1997). All the CCN are placed in 256 logarithmically spaced bins from 0.01 μm to 1 mm. The particles do not move out of their original bins, but the bin size increases as the drops grow, so all droplets in each bin grow at the same rate. Condensation is calculated with the Fukuta and Walter (1970) representation, with a condensation coefficient of 0.04 and an accommodation coefficient of 1.0.

The time steps in the condensation model are smaller than those used to calculate the cloud model trajectories, but interpolation in time is used to match the velocities and thermodynamic properties of the condensation model to those of the cloud model along a prescribed trajectory. The procedures used at each time step in the condensation model are as follows:

(i) the updraft speed at the current location is used to find the new altitude (z);

(ii) droplets in each bin grow using the previous value of the supersaturation, (giving new water vapor and cloud water mixing ratios), and new drops are activated if the supersaturation exceeds its previous maximum;

(iii) dp/dz is calculated from the trajectory to find the new pressure (thus matching any nonhydrostatic pressure variations along the trajectory);

(iv) a dilution factor to correct for the pressure change is calculated and applied to the cloud drop concentration (N) as

$$N_z = \frac{N_{z-\Delta z}\ p_z}{p_{z-\Delta z}} \quad ;$$

(v) the decrease in water vapor pressure that results from the cumulative effects of the droplet growth and the ascent of the parcel is calculated;

(vi) from values of wet equivalent potential temperature θ_q and total water mixing ratio r_t for the parcel, and from corresponding values of θ_q* and r_t* for entrained air (assumed to originate from environmental air at the same pressure level), the mixing fraction α of environmental air required to match the prescribed θ_q' from the cloud model is calculated using

$$\Theta_q{}' = (1-\alpha)\Theta_q + \alpha\Theta_q{}^* \quad ,$$

and this value of α is used to solve for the new value of total water mixing ratio r_t for the parcel using

$$r_t{}' = (1-\alpha)r_t + \alpha r_t{}^* \quad ;$$

(vii) an adjustment is made for evaporation or condensation that would occur due to entrainment and mixing under the assumption that the mixing is "homogeneous" (i.e., no droplet growth or evaporation occurs while mixing produces uniformity in the parcel) by using the mixing fraction α to reduce the new droplet

concentration by dilution according to

$$N' = (1-\alpha) N \quad ;$$

(viii) the equation for θ_q is used to solve iteratively for the temperature T:

$$T = \Theta_q \left(\frac{p-e}{p_o} \right)^{\frac{R_d}{C_t}} \exp\left(\frac{L_v r_v}{C_t T} \right) \quad ,$$

where p_o= 1000 mb, R_d is the dry air gas constant, L_v is the latent heat of vaporization, r_v is the water vapor mixing ratio and C_t is given by

$$C_t = C_{pd} + C_w r_t \quad ,$$

where C_{pd} is the specific heat for dry air at constant pressure, C_w is the specific heat of water and r_t is the total water vapor mixing ratio;

(ix) the resulting temperature and vapor pressure are used to calculate the supersaturation or subsaturation for the next time step.

The cloud properties along the trajectory passed to the condensation model reflect the effects of entrainment and mixing. Because these properties do not uniquely define the amount of environmental air that has mixed with the cloud (only the end result), it is necessary to make an assumption about the source of the entrained air in step (vi) above. To decide the source of the entrained air, Paluch diagrams (Paluch 1979) for the modeled cloud (Fig. 1) were created. The plotted curves at different levels (only one level is presented here) show that the source of the entrained air at any given height in the cloud is near or a small distance above that height, as also found in the Montana cumulus observations studied by Blyth et al. (1988). Based on this evidence, the condensation model assumes that entrained air originates from the same pressure level in the environment.

The drop size distributions for an ensemble (typically 500) of such trajectories, all originating at the same point in the cloud, are then averaged (using 0.04 μm bins) to produce the resulting drop size distribution. This is equivalent to randomly picking individual drops from the different trajectories to form the final size distribution for a particular realization, and averaging over many realizations.

Sedimentation is currently not considered in the calculation of the trajectories. Individual trajectories calculated with the drop terminal velocity included show that the end result is a difference in final position of ~ 5 m, which is much smaller than the cloud model grid spacing of 50 m and is thus neglected. The effect of including sedimentation would broaden the drop size distributions even more, because the larger drops with larger fall speeds would take a longer time to reach the source point (thus allowing for more time for growth), while the smaller drops would have a shorter time to reach the source point and less time for growth.

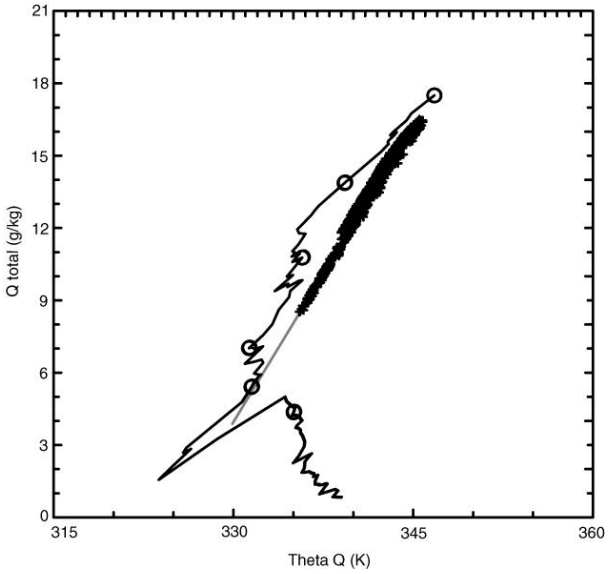

Figure 1. Paluch diagram for the simulated cloud at 4025 m. Sounding is solid black line, with heights in 1 km intervals marked by open circles. Gray line illustrates source region of entrained air. Height of cloud base is 1050 m; height of cloud top at this time is 4500 m.

3. RESULTS

Five different "source points" have been selected, occurring at different times and locations in the simulated cloud (Figs. 2 and 3). The source points are all in regions that have undergone some entrainment, but for case 5 the amount of entrainment is very small. The plotted trajectory paths contain loops from the flow around the back side of the main thermal circulation, or small eddies near the cloud edges. For case 5, all the trajectories are quite similar and smooth, because the particles have stayed ahead of the main thermal, and have not been swept around in its wake.

Figure 4 shows the resulting size distributions arising from the trajectories for all 5 cases, along with a size distribution calculated along one of the trajectories in case 5 with entrainment suppressed (i.e., an adiabatic parcel calculation with velocity matched to the trajectory). The size distributions arising from the entrainment−induced variations of supersaturation among the trajectories are clearly much broader than that for adiabatic ascent, and even produce substantial numbers of drops larger than those calculated for adiabatic ascent. There is a notable lack of small droplets in the modeled distributions, and this is presumably because no new CCN from entrained air are included in the calculations. If this effect were included, more small droplets would be produced and the width of the size distributions would be even greater.

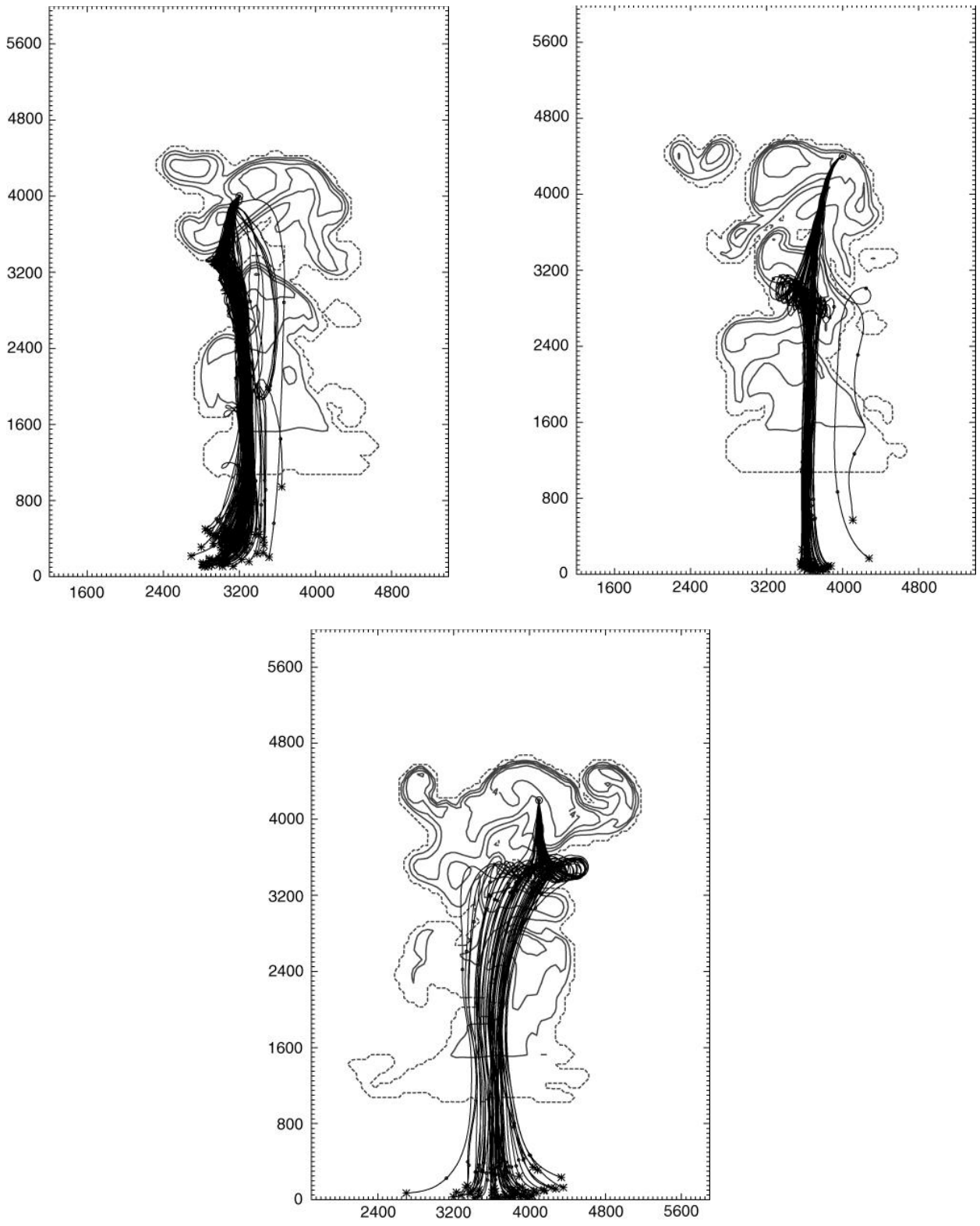

Figure 2. Vertical cross−sections of the simulated cloud at with trajectories overlaid for case 1 (upper left), case 2 (upper right) and case 3 (bottom). Contour interval is 1 g m^{-3} of liquid water content, except for dashed contour denotes 0.001 g m^{-3}. Trajectory starting points are denoted by asterisks, and end point is denoted by bulls−eye. Only a small subset of the total number of trajectories for each case are plotted.

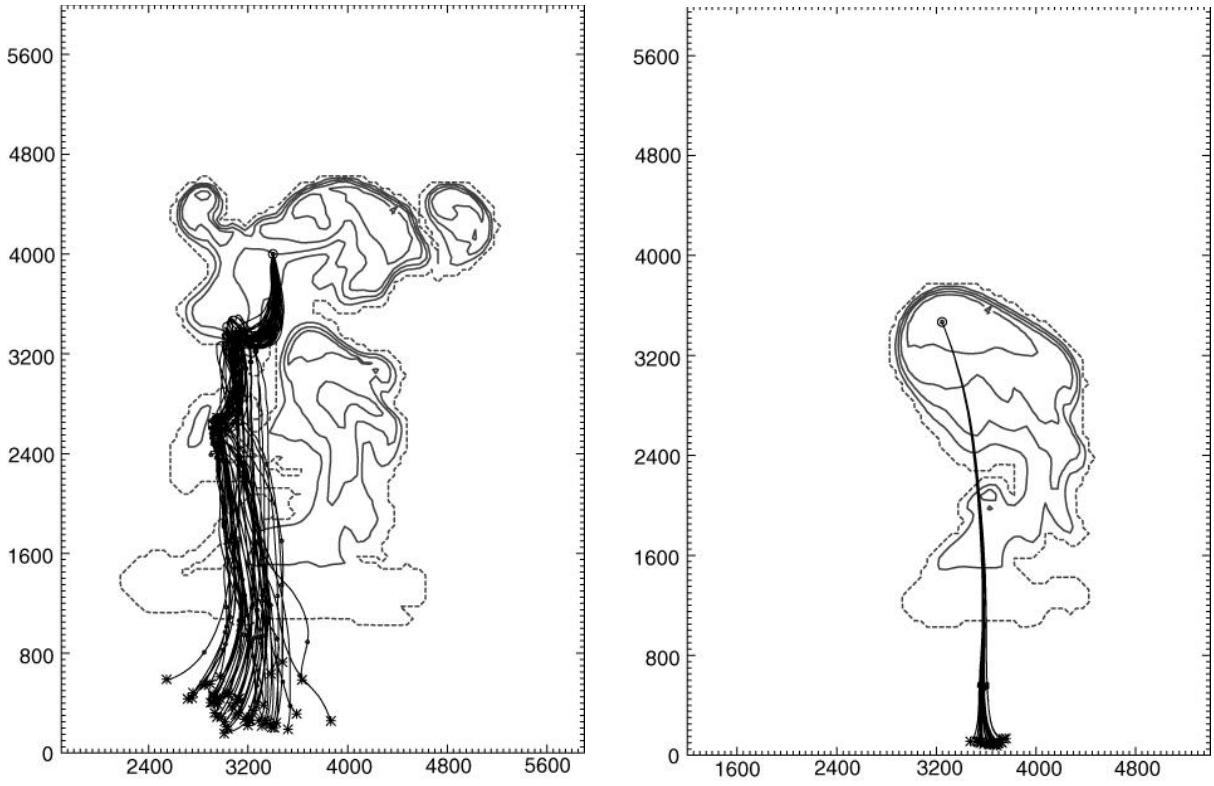

Figure 3. As in Fig. 2, except for case 4 (left) and case 5 (right).

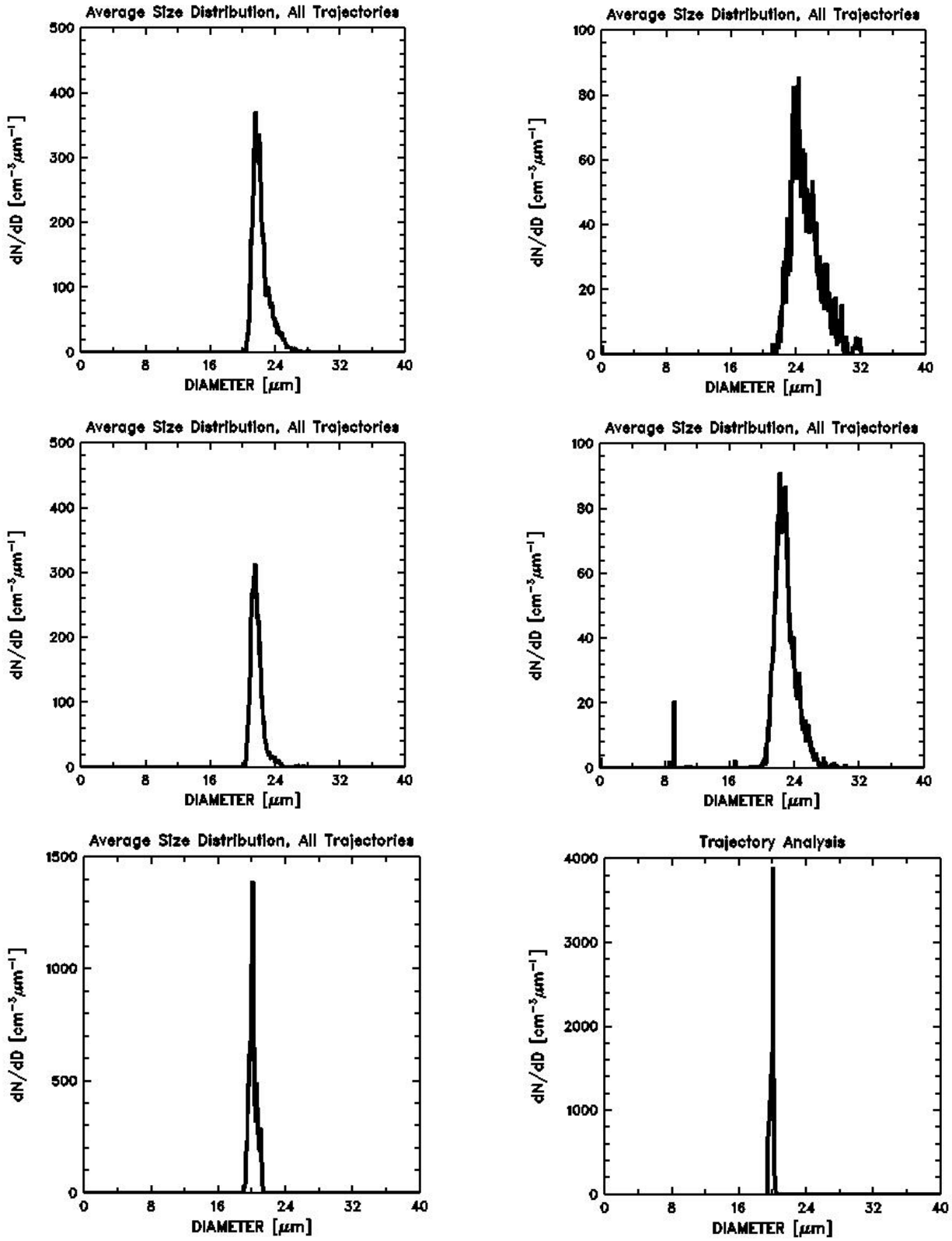

Figure 4. Size distributions resulting from averaging over individual size distributions produced by condensation calculations along each trajectory for case 1 (upper left), case 2 (upper right), case 3 (center left), case 4 (center right) and case 5 (bottom left). A size distribution arising from ascent along one trajectory from case 5 with entrainment suppressed is also shown (bottom right).

Table 1 presents details of the size distributions for the 5 cases, as well as the case for adiabatic ascent. The effect of entrainment in the simulated cloud causes substantial decreases in the total number concentration and liquid water content of the size distributions. The entrainment generally increases the mean diameter of the distributions, presumably because the decrease in the total droplet number due to dilution and evaporation reduces the competition among the droplets for the available water vapor. The entrainment also generally increases the width of the distributions. The relationship between the amount of entrainment (as implied by the liquid water content) and the mean diameter or distribution width is not a strictly linear one, reflecting the stochastic nature of the processes being modeled.

Table 1. Characteristics of the drop size distributions for all cases, 1−5, and the adiabatic case (A). Column headings from left to right denote total drop concentration (cm^{-3}), mean diameter (μm), standard deviation (μm) and liquid water content of the average distribution ($g\ m^{-3}$).

Case	N	$\langle d \rangle$	σ_d	lwc
4	217	22.98	1.37	1.39
2	255	25.25	1.86	2.19
3	427	21.76	0.79	2.31
1	606	22.28	1.07	3.53
5	896	20.17	0.44	3.86
A	1000	19.89	0.23	4.12

Preliminary comparisons with the observed size distributions from the 22 July SCMS cases show that the widths of the modeled size distributions are of the same magnitude as those observed.

4. CONCLUSIONS AND FUTURE WORK

The results of this study demonstrate that variations in supersaturation histories arising from entrainment and mixing in the cloud can result in droplet size variations similar to those often observed in clouds. Drop sizes larger than those calculated from pure adiabatic ascent are also produced in these calculations, but may be unrealistic because of an underestimation of small drops as a result of no new CCN being entrained.

Limitations of this work include the neglect of new CCN being brought into the cloud during entrainment events, the lack of a representation of the intermittent nature of the turbulence, and a lack of representation of inhomogeneous mixing. The homogeneous representation of mixing has a smaller effect on the droplet size distributions than would an inhomogeneous process where not all droplets are subject to the same effects of evaporation following entrainment. Additional work pertaining to inhomogeneous mixing, activation of entrained CCN, and comparison to observations is currently underway.

This study has promising implications for coalescence initiation. Future work will also include an investigation of the largest droplets formed by condensation in the distributions, rather than the width of the peak which is the focus of this study, to see if their sizes and number could explain the rapidity with which the coalescence process appears to be initiated in nature. A realistic representation of sedimentation in the model will be necessary for such a study.

Acknowledgments
The present work was funded by the National Science Foundation, ATM 9981937.

5. REFERENCES

Bartlett, J. T., and P. R. Jonas, 1972: On the dispersion of the sizes of droplets growing by condensation in turbulent clouds. *Quart. J. Roy. Meteor. Soc.,* **98**, 150−164.

Carpenter, R. L., Jr., K. K. Droegemeier, and A. M. Blyth, 1998: Entrainment and detrainment in numerically simulated cumulus congestus clouds. Part I: General results. *J. Atmos. Sci*., **55**, 3417−3432.

Cooper, W. A., 1989: Effects of variable droplet growth histories on droplet size distributions. Part I: Theory. *J. Atmos. Sci*., **46**, 1301−1311.

_____, R. T. Bruintjes and G. K. Mather, 1997: Calculations pertaining to hygroscopic seeding with flares. *J. Appl. Meteor*., **36**, 1449−1469.

Fukuta, N., and L. A. Walter, 1970: Kinetics of hydrometeor growth from a vapor−spherical model. J. Atmos. Sci., 27, 1160−1172.

Klemp, J. B., and R. B. Wilhelmson, 1978: The simulation of three−dimensional convective storm dynamics. *J. Atmos. Sci.*, **35**, 1070−1096.

Lasher−Trapp, S. G., C. A. Knight and J. M. Straka, 2001: Early radar echoes from ultragiant aerosol in a cumulus congestus: Modeling and observations. *J. Atmos. Sci*., **58**, 3545−3562.

Paluch, I. R., 1979: The entrainment mechanism in Colorado cumuli. *J. Atmos. Sc*i., **36**, 2467−2478.

Rodi, A. R., 1981: Studies of the fine scale structure of cumulus clouds. Ph.D. Dissertation, University of Wyoming, Laramie, WY, 328 pp.

Soong, S., and Y. Ogura, 1973: A comparison between axisymmetric and slab−symmetric cumulus cloud models. *J. Atmos. Sci*., **30**, 879−893.